Published online 13 June 2023

NAR Cancer, 2023, Vol. 5, No. 3 **1**
https://doi.org/10.1093/narcan/zcad029

Synthetic lethal interaction between WEE1 and PKMYT1 is a target for multiple low-dose treatment of high-grade serous ovarian carcinoma

Jan Benada[1], Daria Bulanova[1], Violette Azzoni[1], Valdemaras Petrosius[1,2], Saba Ghazanfar[1], Krister Wennerberg[1] and Claus Storgaard Sørensen[1,*]

[1]Biotech Research and Innovation Centre, University of Copenhagen, Ole Maaløes Vej 5, 2200 Copenhagen N, Denmark and [2]Department of Biotechnology and Biomedicine, Technical University of Denmark, Søltofts Plads 224, 2800 Kgs Lyngby, Denmark

Received March 31, 2023; Revised May 24, 2023; Editorial Decision May 29, 2023; Accepted May 31, 2023

ABSTRACT

Ovarian cancer is driven by genetic alterations that necessitate protective DNA damage and replication stress responses through cell cycle control and genome maintenance. This creates specific vulnerabilities that may be exploited therapeutically. WEE1 kinase is a key cell cycle control kinase, and it has emerged as a promising cancer therapy target. However, adverse effects have limited its clinical progress, especially when tested in combination with chemotherapies. A strong genetic interaction between WEE1 and PKMYT1 led us to hypothesize that a multiple low-dose approach utilizing joint WEE1 and PKMYT1 inhibition would allow exploitation of the synthetic lethality. We found that the combination of WEE1 and PKMYT1 inhibition exhibited synergistic effects in eradicating ovarian cancer cells and organoid models at a low dose. The WEE1 and PKMYT1 inhibition synergistically promoted CDK activation. Furthermore, the combined treatment exacerbated DNA replication stress and replication catastrophe, leading to increase of the genomic instability and inflammatory STAT1 signalling activation. These findings suggest a new multiple low-dose approach to harness the potency of WEE1 inhibition through the synthetic lethal interaction with PKMYT1 that may contribute to the development of new treatments for ovarian cancer.

GRAPHICAL ABSTRACT

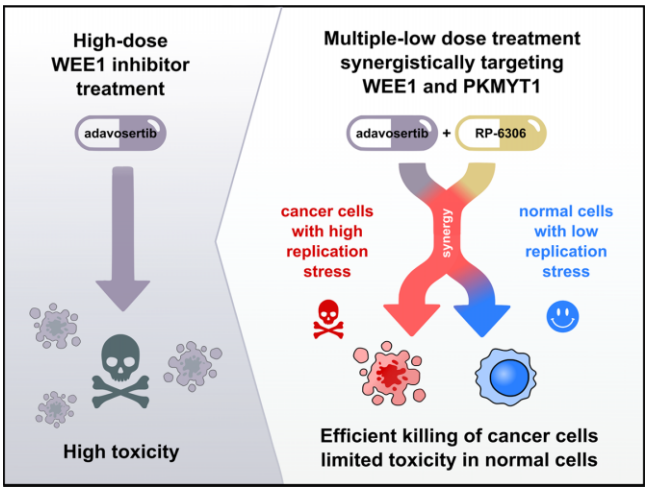

INTRODUCTION

High-grade serous carcinoma (HGSC) is both the most prevalent and most fatal subtype of ovarian cancer. Standard therapy for HGSC consists of cytoreductive surgery, followed by chemotherapy with DNA-damaging agents, such as platinum drugs, either alone or in combination with taxane drugs (1,2,3). While primary tumours usually respond favourably to the treatment, over 80% of cases relapse and more than half of these acquire resistance to the treatment. Moreover, the relapsed HGSC is typically fast-growing and invasive (1,2,3). Platinum-resistant tumours are subjected to salvage therapy with DNA-damaging drugs, including doxorubicin, topotecan, etoposide, vinorelbine and gemcitabine. Nonetheless, the response rate at this stage is only ∼10–15% with a median progression-free survival of 3–4 months, underscoring the urgent need for better treatments (1,2,3). Recently, targeted maintenance treatment with the angiogenesis inhibitor

*To whom correspondence should be addressed. Tel: +45 3532 5678; Email: claus.storgaard@bric.ku.dk

bevacizumab and the poly(ADP-ribose) polymerase (PARP) inhibitors has demonstrated benefits to ovarian cancer patients, even when accounting for the adverse effects associated with treatment (4). However, intrinsic or acquired resistance to PARP inhibitors occurs in most HGSC patients, ultimately limiting the efficacy of this approach (5).

A proposed therapeutic option for HGSC is the use of WEE1 inhibitors (6). WEE1 catalyses inhibitory phosphorylation on tyrosine 15 of both CDK1 and CDK2 and thus limits the CDK activity (7,8). WEE1 inhibition deregulates CDK activity and exacerbates DNA replication stress to intolerable levels, effectively killing the cells in the process termed replication catastrophe (9,10). Mechanistically, unrestricted CDK activity leads to excessive replication origin firing, which in turn results in depletion of protective replication protein A (RPA). RPA exhaustion marks a point of no return, when unprotected replicons collapse in lethal genome-wide DNA breakage (9,11). Moreover, WEE1 inhibition also overrides the G2/M DNA damage checkpoint forcing cells to enter mitosis with unrepaired DNA, which triggers cell death (12). Stringent G2/M checkpoint control is especially vital for cancer cells, as they frequently lose the ability to arrest their cell cycle and repair DNA in the G1 DNA damage checkpoint (13,14).

The most studied inhibitor of WEE1 is adavosertib (AZD1775, MK1775), which has been the focal point of multitude clinical studies (15) (ClinicalTrials.gov). In particular, positive outcomes for HGSC were reported in phase II clinical trials by combining adavosertib and gemcitabine treatment, exploiting high levels of replication stress in HGSC (6). However, despite the years of testing, adavosertib has not reached clinical use, which is mainly due to significant adverse effects when used in combination with chemotherapy (16,17). Of note, several other WEE1 inhibitors are currently evaluated in clinical trials, including ZN-c3 (Zentalis), Debio0123 (Debiopharm), IMP7068 (Impact Therapeutics) and SY4835 (Shouyao Holding) (ClinicalTrials.gov).

An attractive strategy to limit unacceptable toxicity is to use a lower dose of inhibitors but at same time target multiple proteins of a single signalling pathway to still achieve a complete pathway inhibition. This multiple low-dose therapy also reduces cancer selective pressure against a single target that may result in treatment resistance (18,19,20). A prime candidate for synergistic effect with WEE1 is the kinase PKMYT1. PKMYT1 phosphorylates CDK1 at threonine 14 and thus inhibits CDK activity (21). WEE1 and PKMYT1 have been originally described to be synthetically lethal in fission yeast (22,23). The synthetic lethal interaction has been further confirmed in CRISPR–Cas9 screens in human cancer cells (24). Moreover, upregulation of PKMYT1 has been shown to promote resistance of cancer cells to WEE1 inhibition (25).

PKMYT1 as an anticancer target is much less studied than WEE1; however, Repare Therapeutics has recently identified a first-in-class PKMYT1 inhibitor, RP-6306 (26). RP-6306, used as single compound, showed promising *in vitro* results for ovarian cancer cells (27), and is currently being fast tracked to clinical trials (ClinicalTrials.gov; NCT05147350, NCT05147272, NCT04855656, NCT05605509 and NCT05601440). Notably, PKMYT1 expression was reported to be upregulated in ovarian cancers and correlated with poor prognosis, making it an appealing therapeutic target (28). The availability of a PKMYT1 inhibitor prompted us to investigate the synergistic potential of its combined application with WEE1 inhibition.

MATERIALS AND METHODS

Cell lines

Human osteosarcoma cell lines U2OS (ATCC) and COV362 (ATCC) were cultured in Dulbecco's modified Eagle's medium (DMEM; Gibco) supplemented with 10% foetal bovine serum (FBS; Cytiva) and 1% penicillin–streptomycin (10 000 U/ml; Gibco). High-grade serous ovarian cancer cell lines OVCAR3, OVCAR8 (NCI Tumor Repository, Frederick, MD) and KURAMOCHI (Japanese Collection of Research Bioresources Cell Bank) were cultured in Roswell Park Memorial Institute 1640 medium (Gibco) supplemented with 10% FBS and 1% penicillin–streptomycin. BJ fibroblast HRAS(G12V) Tet ON cells were cultured in DMEM (Gibco) supplemented with 10% Tet-System Approved FBS (Gibco) and 1% penicillin–streptomycin (10 000 U/ml; Gibco). HRAS(G12V) expression was induced by 2 μg/ml of doxycycline. All cells were cultured at 37°C with 5% CO_2 and checked for mycoplasma infection regularly.

Organoid cultures

Long-term HGSC organoid cultures were established and characterized earlier as described (29). The samples were cultured in 7.5 mg/ml BME-2 matrix (Cultrex, BioTechne) in sample-specific media (29)—for EOC883 and EOC172, Medium 1 [Advanced DMEM/F12 (#12634010, Gibco), supplemented with 100 μg/ml Primocin (#ant-pm-1, InvivoGen), 10 mM HEPES (#15630080, Gibco), 1 mM *N*-acetylcysteine (#A7250, Sigma), 1× GlutaMAX (#35050061), 1× B-27 Supplement, 0.5 μM SB202190 (#HY-10295, MedChemExpress), 0.5 μM A83-01 (#SML0788, Sigma), 10 ng/ml recombinant human FGF-10 (#100-26, PeproTech), 10 ng/ml recombinant human FGF-4 (#100-31, PeproTech), 100 nM β-estradiol (#E2758, Sigma) and 5 mM nicotinamide (#N0636, Sigma)]; for EOC989, EOC540 and EOC382, Medium 2 (Medium 1 supplemented with 5 ng/ml EGF, 5 μM heregulin-1β, 0.5 μg/ml hydrocortisone and 5 μM forskolin).

Organoid drug sensitivity assay

The organoids were dissociated in TrypLE Express solution (Thermo Fisher) as described previously (35). Dissociated cells were resuspended in 7.5 mg/ml BME-2 matrix gel at 2–5 × 10^4 cells/ml and seeded in 10 μl droplets to individual wells of 96-well CellCarrier Ultra plates (PerkinElmer). Once settled, 200 μl of the organoid-specific growth medium containing 5 μM ROCK inhibitor Y-27632 (HY-10583, MedChemExpress) was added. After 4 days, the growth medium was changed to 200 μl of medium

containing adavosertib or RP-6306 at the indicated concentrations, or 25 μM staurosporine as a positive control for cytotoxicity. After 7 days, organoids were stained using Hoechst 33342 (1 μg/ml) and CellTox Green (Promega, 1/20 000) dyes for 8 h prior to imaging at an Opera Phenix (PerkinElmer) confocal screening microscope. The fraction of dead organoids was discriminated by the CellTox Green signal per organoid from the confocal images analysis using Harmony software (PerkinElmer).

Drug sensitivity assay

Drugs diluted in dimethyl sulfoxide (DMSO) to the desired concentrations were dispensed at 30 nl volume to 384-well black plates (Corning, cat#3864) using an Echo 550 acoustic liquid handler (Labcyte). Cell killing benzethonium chloride (100 μM) and compound vehicle (DMSO, 0.1%) were used as positive and negative controls, respectively. Cells were diluted to medium at the desired number per ml and the suspension was dispensed to the predrugged plates at 30 μl. Alternatively, drugs were dispensed by manual pipetting into 96-well plates (Greiner-BIO) and cells were dispensed at the desired number at 100 μl. After 5 days of incubation at 37°C, 10 μl/30 μl for 384-well/96-well plates, respectively, of phosphate-buffered saline (PBS) containing 4 μg/ml Hoechst 33342 and 1/10 000 CellTox Green dyes was added for 1 h prior to imaging. Images were obtained automatically with the ScanR acquisition software controlling a motorized Olympus IX-83 wide-field microscope, equipped with a Lumencor SpectraX light engine and Hamamatsu ORCA-FLASH 4.0, using an Olympus Universal Plan Super Apo 4×/0.16 AIR objective.

Quantitative image-based cytometry

Cells growing on either 96-well microplates (Greiner-BIO) or 12 mm coverslips were treated with different combinations of drugs for indicated time intervals. After the treatment, the medium was quickly removed and the cells were incubated in pre-extraction buffer (25 mM HEPES, pH 7.5, 50 mM NaCl, 1 mM EDTA, 3 mM $MgCl_2$, 300 mM sucrose and 0.5% Triton X-100) on ice for 2 min and immediately fixed in formaldehyde 4% (VWR) for 10 min at the room temperature. For the analysis of the micronuclei number and cGAS, the pre-extraction step was omitted. Primary antibodies (γH2AX 1:300, Cell Signaling Technology, cat#2577; RPA 1:300, Millipore, cat#MABE285; FOXM1pT600 1:1000, Cell Signaling Technology, cat#14655; cGAS 1:300, Cell Signaling Technology, cat#15102) were diluted in filtered DMEM containing 10% FBS and 5% bovine serum albumin (BSA; Sigma). Incubations with the primary antibodies were performed at room temperature for 1 h. Microplates were washed three times with 0.05% PBS–Tween 20 and incubated in DMEM/FBS/BSA containing secondary fluorescently labelled antibodies (Alexa Fluor dyes 1:1000; Thermo Fisher Scientific) and DAPI (0.5 mg/ml; Sigma–Aldrich) for 1 h at room temperature. Images were obtained automatically with the ScanR acquisition software controlling a motorized Olympus IX-83 wide-field microscope, equipped with a Lumencor SpectraX light engine and Hamamatsu ORCA-FLASH 4.0. Olympus PlanC N 10×/0.25 AIR objective was used to capture γH2AX, RPA and quantitative image-based cytometry (QIBC) data. Micronuclei images were obtained with a 0.75 AIR UPlanSApo 40×/0.95 AIR objective. Images were processed and quantified using the ScanR image analysis software for total nuclear pixel intensities for DAPI (arbitrary units: AU) and mean (total pixel intensities divided by nuclear area) nuclear intensities (AU) for γH2AX, chromatin-bound RPA and FOXM1pT600. Micronuclei were segmented based on DAPI channel within a cytoplasmic mask surrounding the nucleus. Similarly, cGAS intensity was determined within the cytoplasmic mask. Further analysis and data visualization was then carried out with Tibco Spotfire software (Tibco, RRID:SCR_008858). Representative images were processed using ImageJ/Fiji (RRID:SCR_002285, https://imagej.net/).

Western blotting

Cells were lysed in RIPA (Sigma) buffer containing EDTA-free protease inhibitor cocktail (Roche) and phosphatase inhibitors (Roche). Lysates were treated with benzonase nuclease (Sigma–Aldrich) for 30 min on ice. Lysates were centrifuged for 15 min at 20 000 × *g* at 4°C. Protein concentration was then measured with the Bradford assay and adjusted accordingly to ensure equal loading. Lysates were mixed with 4× Laemmli sample buffer (Sigma) and boiled for 10 min at 95°C. Samples were run on NuPAGE Bis-Tris 4–12% gels according to manufacturer's instructions. Proteins were then transferred to a nitrocellulose membrane and blocked with PBS + 0.1% Tween 20 + 5% milk powder (Sigma) and incubated overnight with primary antibodies at 4°C. The membrane was then washed 3 × 5 min in PBS + 0.1% Tween 20 and incubated with secondary HRP conjugated antibodies for 2 h at room temperature. Membranes were again washed 3 × 5 min with PBS + 0.1% Tween 20 and incubated with Classico/Crescendo Western HRP substrate (MilliporeSigma) for 2 min. Chemiluminescence signal was detected using a Bio-Rad ChemiDoc Touch Imaging System. The following primary antibodies were used: STAT1pY701 1:100, Cell Signaling Technology, cat#9171; STAT1 1:1000, Cell Signaling Technology, cat#9176; Vinculin 1:10 000, Sigma, cat#V9131; CDK1 1:1000, Abcam, cat#ab18; CDK1pT14 1:1000, Abcam, cat#ab58509; CDK1pT15 1:1000, Cell Signaling Technology, cat#9111S; phospho-CDK substrate motif 1:1000, Cell Signaling Technology, cat#9477; CHK2 1:500, Santa Cruz, cat#sc-56296; CHK2pT18 1:500, Cell Signaling Technology, cat#2661; CHK1 1:500, Santa Cruz, cat#sc-56291; CHK2pS345 1:500, Cell Signaling Technology, cat# 2348; γH2AX 1:1000, Cell Signaling Technology, cat#2577; RPA70 1:1000, Abcam, cat#ab79398; TBK1pS172 1:200, Cell Signaling Technology, cat#5483; TBK1 1:500, Cell Signaling Technology, cat#38066; Actin 1:20000, Millipore, cat#MAB1501.

Cell fractionation

Cells were grown in 10 cm dishes, treated as indicated, washed three times with ice-cold PBS and harvested. The

soluble fractions were extracted by incubation in ice-cold nuclear buffer (10 mM HEPES, pH 7, 200 mM NaCl, 1 mM EDTA, 0.5% NP-40) supplemented with protease and phosphatase inhibitors (Roche) for 10 min on ice and centrifuged at 2000 × *g* for 6 min. The remaining pellet was rinsed once with ice-cold washing buffer (10 mM HEPES, pH 7, 50 mM NaCl, 0.3 M sucrose, 0.5% Triton X-100) supplemented with protease and phosphatase inhibitors (Roche), which was removed by centrifugation at 1400 × *g* for 6 min. Chromatin fractions were extracted by incubation in RIPA buffer (50 mM Tris–HCl, pH 8, 150 mM NaCl, 1% IGEPAL CA-630, 0.1% SDS, 0.1% sodium deoxycholate) supplemented with protease and phosphatase inhibitors (Roche) and benzonase nuclease (Sigma) for 30 min on ice and clarified by centrifugation at maximum speed.

Drug–drug interaction analysis

To assess the outcome of the drug combination treatment, we applied the zero interaction potency (ZIP) synergy model (30). The ZIP score reflects the additional cell line response induced by the combinatorial treatment compared to the expected response based on the two single compounds. A ZIP score ≥ 10 is considered synergistic and a score ≤ -10 represents antagonism. ZIP scores were calculated for each combination in the dose matrix by SynergyFinder 2.0 (31) (https://synergyfinder.org/ and https://synergyfinder.fimm.fi) and plotted as synergy landscapes using RStudio (RRID:SCR_000432, https://www.r-project.org) and ggplot2 package (https://ggplot2.tidyverse.org) (32).

Statistical analysis

Statistical analyses were conducted using GraphPad Prism (v.9.5.1). For multiple comparisons, statistical significance (adjusted *P* values) was calculated using the two-way analysis of variance (ANOVA), Tukey multiple comparison test, Welch ANOVA test with Dunnett's multiple comparison test or unpaired Student's *t* test. Results are reported as non-significant at $P > 0.05$, and with increasing degrees of significance symbolized by the number of asterisks: (*) $0.01 < P \leq 0.05$, (**) $0.001 < P \leq 0.01$, (***) $0.0001 < P \leq 0.001$ and (****) $P \leq 0.0001$. Statistical details for each experiment can be found in the corresponding legend.

In vivo drug tolerance study

All experiments were carried out under authorization and guidance from the Danish Inspectorate for Animal Experimentation under license number 2021-15-0201-00993, the animal use protocol number P22-560 specifically applicable to the experiments described in the study. Female 7-week-old mice of NGX (NOD-Prkdc scid-IL2rg Tm1/Rj) strain (Janvier Labs) were randomized in four treatment cohorts of six animals. The mice were housed in individually ventilated cages with a humidity of 55% ± 10%, a temperature of 22 ± 2°C and a dark/light cycle of 12 h/12 h with light from 6:00 to 18:00. Adavosertib (Repare Therapeutics) and RP-6306 (Repare Therapeutics) were formulated in 1% DMSO and 0.5% methylcellulose and administered by oral gavage at 15 and 5 mg/kg, respectively, alone or in combination. For intermittent 21-day dosing, the drugs, the combination or the vehicle was given twice daily, with 8 h interval, for 5 days a week, followed by 2 treatment-free days. Animal weight was measured twice weekly, and the overall animal condition was monitored daily. At the end of the treatment, all mice were humanely sacrificed and liver weights were measured.

Pharmacokinetics

Whole blood samples were collected 30 min and 8 h after the first drug treatment. Immediately after collection, 20 μl of blood was mixed with 60 μl of 0.1 M citrate buffer (0.1 M trisodium citrate, pH 7.4) and stored at –80°C before the analysis. All samples were quantified using a reversed-phase liquid chromatography gradient coupled to electrospray mass spectrometry operated in positive mode. Pharmacokinetic parameters were calculated using non-compartmental analysis.

RESULTS

Combined inhibition of WEE1 and PKMYT1 synergizes in killing of cancer cells

WEE1 inhibition has emerged as a strategy to eliminate cancer cells; however, adverse effect concerns have warranted further preclinical investigations. We noted that combined WEE1 and PKMYT1 genetic ablation was lethal in a glioma setting (24). To evaluate the potential synergistic effect of co-targeting WEE1 and PKMYT1, we conducted a dose response matrix for cell viability with the WEE1 inhibitor adavosertib in combination with the PKMYT1 inhibitor RP-6306 (Figure 1A and B). The U2OS cell line was selected as a model since it has been well characterized for WEE1 and CDK functions, and notably, investigated in detail for the effects of adavosertib treatment (33). At 100 nM concentration, the combinatorial treatment led to efficient killing of most U2OS cells (Figure 1B). In stark contrast, treatment with 100 nM of single compound treatment had negligible effect on cell viability (Figure 1B). A synergy analysis revealed a strong synergistic interaction between the inhibitors (Figure 1C). Furthermore, these findings were reproduced using the combination of RP-6306 with another clinically relevant WEE1 inhibitor, ZN-c3 (Supplementary Figure S1A and B). The efficacy of used inhibitors was validated by western blots, assaying the substrates of WEE1 and PKMYT1—CDK1pY15 and CDK1pT14, respectively (Supplementary Figure S1C and D).

In contrast to normal cells, cancer cells are characterized by multiple genetic alterations in driver genes that promote high rate of proliferation and impose replication stress (34,35). The high level of replication stress renders cancer cells particularly dependent on safeguarding mechanisms and these can be exploited by cancer treatments. To assess whether the multiple low-dose application of WEE1i and PKMYT1i preferentially eliminated high replication stress cells and less so their normal counterparts, we conducted dose response matrix in normal BJ fibroblast cells with doxycycline-inducible oncogene HRAS(G12V) (36,37). To

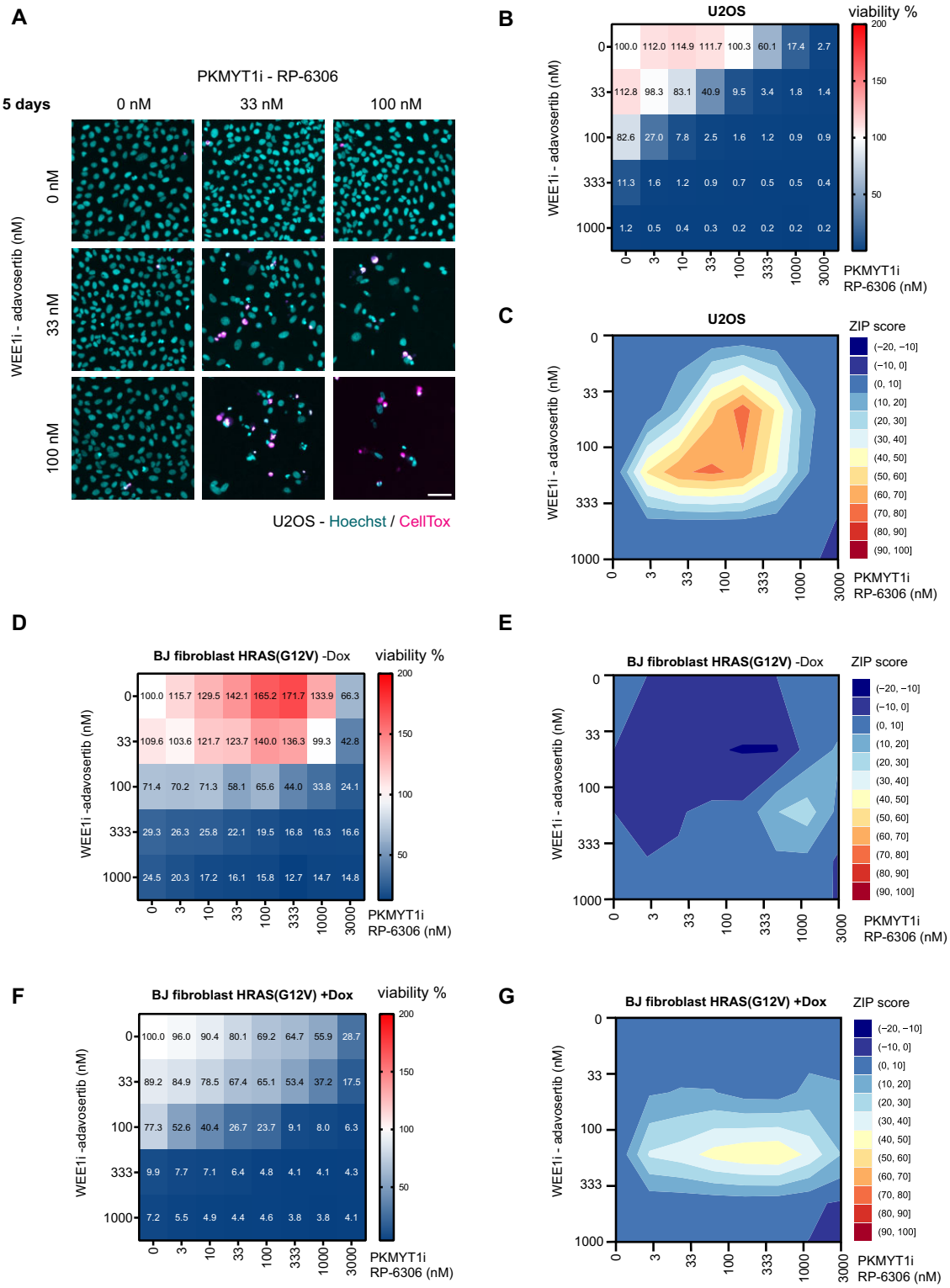

Figure 1. Combined inhibition of WEE1 and PKMYT1 synergizes in killing of cancer cells. (**A**) Representative images of cell viability assay upon 5-day treatment with adavosertib in combination with RP-6306 in U2OS cells; scale bar represents 50 μm. (**B**) Dose response matrix for cell viability upon 5-day treatment with adavosertib in combination with RP-6306 in U2OS cells; data represent mean from triplicate. (**C**) Synergy ZIP scores corresponding to data in panel (B) presented a synergy landscape. A score ≥10 represents synergy and a score ≤−10 represents antagonism. (**D**) Dose response matrix for cell viability upon 5-day treatment with adavosertib in combination with RP-6306 in BJ fibroblast HRAS(G12V) Tet ON cells without doxycycline; data represent mean from triplicate. (**E**) Synergy ZIP scores corresponding to data in panel (D) presented a synergy landscape. (**F**) Dose response matrix for cell viability upon 5-day treatment with adavosertib in combination with RP-6306 in BJ fibroblast HRAS(G12V) Tet ON cells with doxycycline-induced expression; doxycycline has been added 2 days before inhibitor treatment and together with inhibitors; data represent mean from triplicate. (**G**) Synergy ZIP scores corresponding to data in panel (F).

first confirm the impact of HRAS(G12V) induction, we monitored proliferation rates that indeed were elevated by activating HRAS signalling (Supplementary Figure S1E). Moreover, normal non-induced BJ fibroblasts were indeed more resistant to the treatment and exhibited cell death only in higher doses compared to U2OS cells (Figure 1D). This was particularly marked for the response to the PKMYT1 inhibitor. Accordingly, the synergy score was comparably lower in the non-induced setting, and the inhibitors synergized only in a very limited concentration window (Figure 1E). Importantly, HRAS(G12V) induction sensitized the BJ cells to the treatment (Figure 1F and G). To further investigate the impact of combinatorial dosing on normal cells, we administered adavosertib and RP-6306 by oral gavage to mice. The achieved plasma levels (when corrected to plasma protein binding) of both compounds were in a concentration range where we observed synergistic effect in killing cancer cells *in vitro* (Supplementary Figure S2A–C). Notably, compounds had little impact on mouse bodyweight and liver size when administered individually or jointly (Supplementary Figure S2D and E). This suggests that when administered at low doses, the combinatorial dosing is tolerated in mouse models.

WEE1i and PKMYT1i co-inhibition exacerbates replication stress and triggers replication catastrophe

Next, we aimed to characterize in detail the mechanism of action of the WEE1i and PKMYT1i combination. WEE1 and PKMYT1 suppress replication stress, and they also guard against premature mitotic entry even in cells experiencing genotoxic challenges through replication stress (12,27). Thus, we reasoned that combined WEE1i and PKMYT1i could elevate replication stress to intolerable level. To assess replication stress levels, we employed QIBC to measure accumulation of single-stranded DNA by quantifying the levels of chromatin-bound RPA and phosphorylation of histone H2AX on serine 139 (γH2AX) as a marker of DNA damage (9). The dose response matrix of acute treatment (4 h) displayed a synergistic effect of adavosertib and RP-6306 in inducing the replication stress, which in higher inhibitor concentration propagated into replication catastrophe (Figure 2A and B, and Supplementary Figure S3A). We observed the same impact for the combination of ZN-c3 and RP-6306 (Supplementary Figure S3B–D). Given the role of WEE1 and PKMYT1 as master regulators of CDK activity, we reasoned that induction of replication stress and catastrophe corresponded to increased levels of CDK activity in S phase. Indeed, we observed that CDK activity, measured as phosphorylation of the CDK substrate FOXM1 at threonine 600 (38), increased rapidly upon the combined treatment and correlated with induction of replication stress as measured by QIBC (Figure 2C–E). Moreover, we were able to reverse the replication catastrophe phenotype by inhibition of CDK activity with CDK1i RO-3306 (Figure 2C–E) (39). Complementary to QIBC, western blot analysis of cellular fractionates showed increased CDK activity, as measured by pan-CDK substrate, and increased chromatin loading of RPA, which indicates replication stress. Of note, CDK1i RO-3306 moderately inhibits also CDK2 (39). Given this limitation and the overlapping substrates and roles of both CDK1 and CDK2, we refrain to pinpoint the observed effect exclusively to either CDK1 or CDK2, albeit it is clearly driven by CDK activity. We also observed increased phosphorylation and activation of markers of the DNA damage response such as CHK1 phosphorylated at serine 345, CHK2 phosphorylated at threonine 68 and γH2AX (Figure 2F). Collectively, the data indicated a marked replication stress and replication catastrophe response to combined WEE1 and PKMYT1 inhibition that likely explains the major treatment lethality in cancer cells. Moreover, cells that do not die in imminent replication catastrophe will be forced by high CDK activity into premature mitotic entry with high levels of replication stress-generated DNA damage resulting in further loss of cell fitness.

Combined WEE1 and PKMYT1 inhibition increases genomic instability and activates a cGAS-STING response

Increased levels of replication stress have been associated with exacerbation of genome instability and formation of micronuclei after mitotic progression with DNA damage (40,41). To test micronuclei formation in our system, we treated the U2OS cells with combinatorial low-dose WEE1i and PKMYT1i for 3 days and assessed the percentage of cells with micronuclei. We observed a significant increase in their formation with combinatorial WEE1i and PKMYT1i treatment in doses as low as 33 nM (Figure 3A and B). The increased presence of micronuclei is linked to activation of innate immunity and the clearance of tumours *in vivo* (40). Mechanistically, this is mediated by the cGAS-STING pathway and subsequent activation of STAT signalling response. Accordingly, we observed increased accumulation of cGAS (Figure 3A and C), activation of its downstream effector TANK-binding kinase 1 (TBK1pS172) and elevated marker of STAT1 activation (STAT1pY701) (Figure 3D). Taken together, these data demonstrate that the WEE1i and PKMYT1i combination activates cGAS-STING response.

WEE1i and PKMYT1i multiple low-dose treatment is efficient against a variety of HGSC cell lines regardless of driver oncogene

As described above, combined WEE1i and PKMYT1i application might be suited for aggressive hard-to-treat cancers with high proliferation rates, such as HGSC. In addition to high proliferation rate, ovarian cancers almost ubiquitously overexpress PKMYT1, suggesting their dependence on PKMYT1 activity (Supplementary Figure S4A) (25). Also, despite the partially overlapping roles of WEE1 and PKMYT1, we did not observe that their expression would be upregulated in mutually exclusive fashion in tumours (Supplementary Figure S4B), supporting the rationale of combined targeting. To address the efficacy of combined WEE1i and PKMYT1i treatment in HGSC relevant systems, we tested a diverse panel of HGSC cell lines in the dose response matrix for cell viability. These included OVCAR3, OVCAR8, COV318, COV362 and KURAMOCHI cell lines. We previously profiled these cell lines for their expression of driver oncogenes

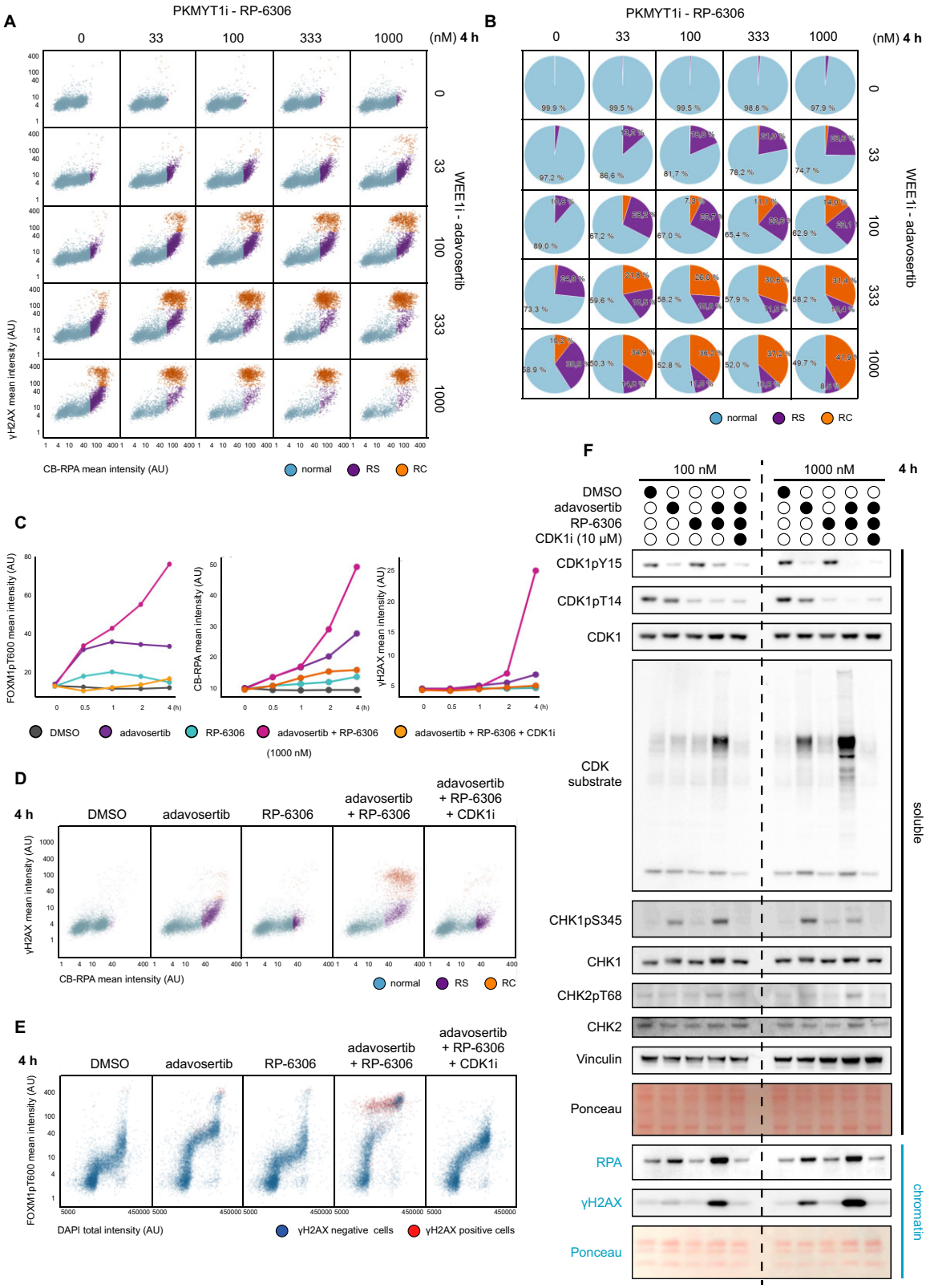

Figure 2. WEE1 and PKMYT1 co-inhibition exacerbates replication stress and triggers replication catastrophe. (**A**) Dose response matrix for QIBC analysis of replication stress upon 4 h treatment with adavosertib in combination with RP-6306 in U2OS cells. AU = arbitrary unit; RS = replication stress; RC = replication catastrophe. (**B**) Analysis of relative cell population percentage from panel (A). (**C**) Line plots for CDK activity (FOXM1pT600), chromatin-bound RPA (CB-RPA) and γH2AX in indicated treatments. (**D**) QIBC plots related to panel (C) for CB-RPA and γH2AX. (**E**) QIBC plots related to panel (C) for FOXM1pT600 and DAPI; red indicates γH2AX-positive cells; AU = arbitrary unit. (**F**) Western blot analysis of soluble and chromatin fractions following indicated treatments of U2OS cells; CDK1i = RO-3306, $n = 2$.

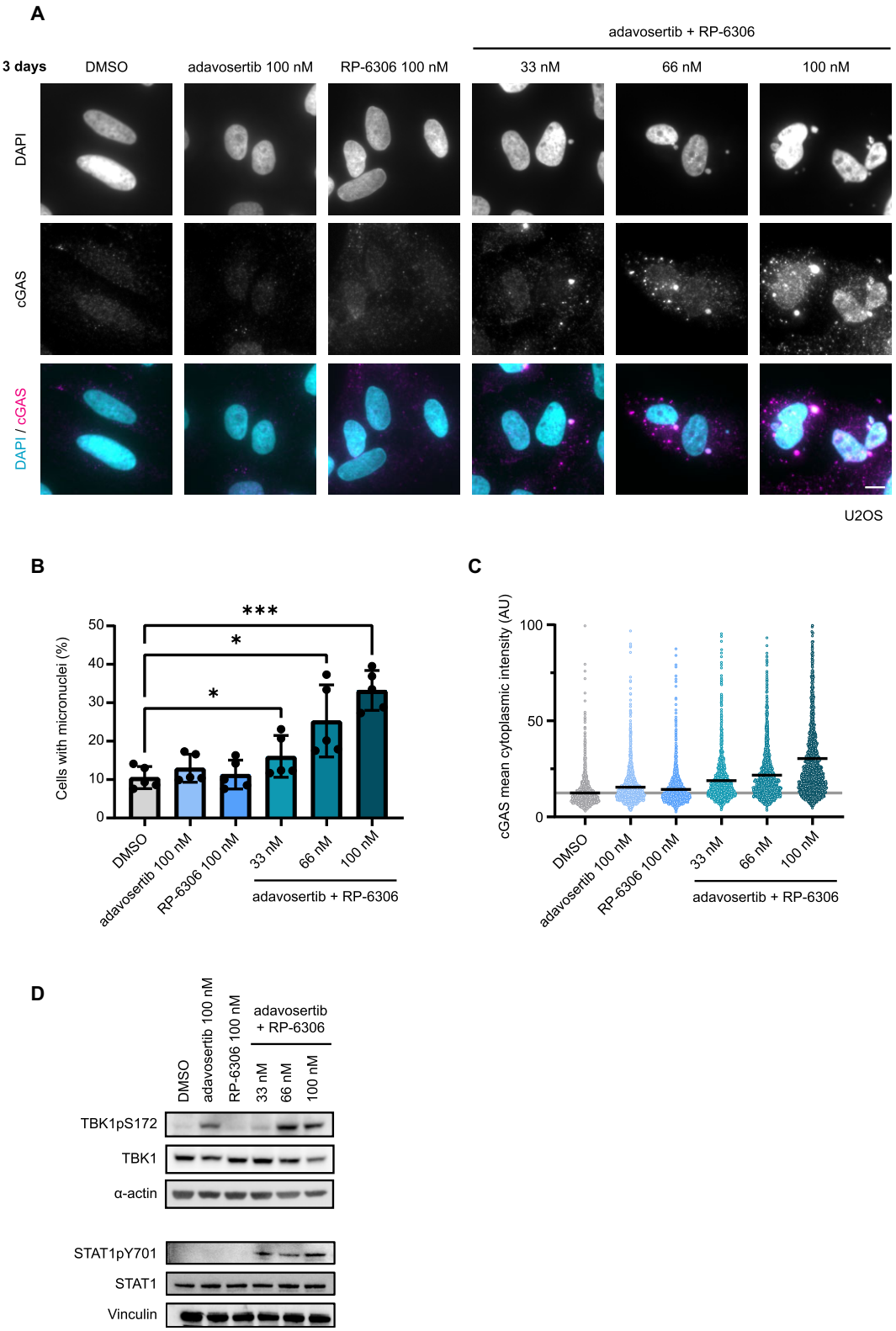

Figure 3. WEE1 and PKMYT1 co-inhibition increases genomic instability and activates cGAS-STING response. (**A**) Representative images of micronuclei formation and cGAS activation upon 3-day treatment with adavosertib in combination with RP-6306 in U2OS cells; scale bar represents 10 μm. (**B**) Quantification of micronuclei formation activation upon 3-day treatment with adavosertib in combination with RP-6306 in U2OS cells; bars indicate mean and SD from biological quintuplicate; two-way analysis of variance (ANOVA): (*) $0.01 < P \leq 0.05$, (**) $0.001 < P \leq 0.01$ and (***) $0.0001 < P \leq 0.001$. (**C**) Quantification of cytoplasmic cGAS intensity upon 3-day treatment with adavosertib in combination with RP-6306 in U2OS cells; bars indicate mean. (**D**) Western blot analysis of TBK1 activation (TBK1pS172) and STAT1 activation (STAT1pY701) upon 3-day treatment with adavosertib in combination with RP-6306 in U2OS cells, $n = 2$.

(Supplementary Figure S4C) (42). Regardless of the expression of specific driver oncogenes, all ovarian cancer cell lines were eradicated by WEE1i and PKMYT1i following multiple low-dose exposure (Figure 4A–J). Upon tailored inspection and like U2OS cells, we observed replication stress and induction of replication catastrophe in OVCAR3 (high cyclin E; Supplementary Figure S5A and B), KURAMOCHI (high KRAS; Supplementary Figure S5C and D) and OVCAR8 (moderately high cyclin E and MYC; Supplementary Figure S5E and F) after the WEE1 and PKMYT1 inhibition in multiple low-dose treatment. We also noted that all tested ovarian cancer cell lines responded in a similar dose range to U2OS, with COV318 displaying slightly different pattern. COV318 represents a highly heterogeneous cell line and the majority of COV318 population responded with even higher sensitivity than the other HGSC cell lines, though ∼10% of the cells survived the treatment. In addition, we recapitulated the findings of increased micronuclei formation and activation of cGAS-STING response from U2OS in the OVCAR8 cell model (Supplementary Figure S6A–D).

WEE1i and PKMYT1i multiple low-dose approach eradicates patient-derived ovarian cancer organoids

To further assess the potential for translation of the WEE1i and PKMYT1i multiple low-dose approach, we evaluated its efficacy in a set of clinically relevant HGSC patient-derived organoid cultures that retained genetic makeup and heterogeneity of the tumour of origin (summarized in Figure 5A) (29). Imaging-based toxicity assay revealed dose-dependent synergistic efficacy of the combination in all tested HGSC organoid cultures (Figure 5B−F), independent of *CCNE1*, *MYC* or *KRAS* amplification, the site of origin of the tumour cells or previous exposure to the replication stress-inducing carboplatin-based neoadjuvant chemotherapy (NACT). Importantly, organoid cultures EOC989 and EOC884, which were derived from residual tumour cells from patients treated with chemotherapy (NACT), showed prominent synergistic response to the combined WEE1 and PKMYT1 inhibition. Both WEE1 and PKMYT1 inhibitors are tested in clinical trials in combination with gemcitabine (ClinicalTrials.gov, NCT02101775 and NCT05147272). Therefore, we also addressed potential impact of combining gemcitabine with our multiple low-dose approach. We pre-treated select ovarian cancer cells (OVCAR3 and KURAMOCHI) and organoids (EOC884 and EOC989) with gemcitabine for 18 h followed by combined WEE1 and PKMYT1 inhibition. We observed a considerable impact as cells were more readily eradicated following gemcitabine pre-treatment (Supplementary Figure S7A−D). This suggests potential in combining standard chemotherapy with the WEE1i and PKMYT1i multiple low-dose approach.

DISCUSSION

Here, we report the combinatorial drugging of PKMYT1 and WEE1 kinases, which synergistically eradicates cancer cells already at low drug dose. Our data highlight the potential for multiple low-dose treatment and support the notion that combining full-dose treatments may not be the only approach when administrating a set of targeted drugs. Synthetically lethal interactions are attractive in cancer treatment as they may allow reduced adverse effects while drugging cancer-specific vulnerabilities in a similar manner as the targeting of BRCA deficiency with PARP inhibition (43). However, few drug candidates and treatments are currently based on synthetic lethality and the multiple low-dose approach is still under development. The multiple low-dose treatment may represent a desirable strategy also for targeting other checkpoint kinases as Golder *et al.* demonstrated that multiple low-dose combinatorial drugging of ATR and CHK1 inhibitors proved effective in killing HGSC cells (44).

Our data show that cancer cells or oncogene exposed cells are more sensitive than normal cells to the WEE1i and PKMYT1i combinatorial treatment, which suggests the evolution of sensitivity during cancer development. It was recently demonstrated that PKMYT1 inhibition with RP-6306 displays synthetic lethality with *CCNE1* amplification based on the marked replication stress induced by CCNE1 overexpression (27). Indeed, cancer cells generally display elevated replication stress due to activated drivers such as *CCNE1*, *KRAS* and *MYC* (34,35). We observed that oncogenic HRAS(G12V) expression also sensitized cells to PKMYT1 inhibition alone and to combined WEE1i and PKMYT1i treatment. In addition, combined WEE1i and PKMYT1i treatment was effective in killing a diverse panel of HGSC cell lines and organoids, regardless of their driver oncogene. This suggests that the treatment efficacy is not limited to a particular oncogene, but rather to a more general feature of oncogene-induced replication stress. In support of this notion, we have observed an exacerbation of replication stress and induction of replication catastrophe, which likely mechanistically underlay a major part of combinatorial treatment lethality in cancer cells. Moreover, cell cycle control in cancer cells is perturbed by the frequent hits in the p53 and retinoblastoma protein (RB) pathways (45). This creates a dependence on the remaining cell cycle control mechanisms and causes cancer cell vulnerabilities to targeted treatments that interfere with these mechanisms. Thus, increased replication stress and limited cell cycle control mechanisms make cancer cells reliant on G2 phase control to limit detrimental premature mitotic entry. Deregulated passage through G2–M transition promotes mitotic cell death and it also triggers micronuclei formation, which in turn leads to innate immunity activation such as cGAS-STING-mediated interferon responses (40,41,46). In agreement with this finding, we observed induced cGAS-STING signalling at low doses of combinatorial treatment. We also observed that the low-dose combination appeared well tolerated in mouse models, although comprehensive additional studies are needed to evaluate the *in vivo* efficacy of the low-dose combination, as well as tolerability in higher species.

The ubiquitous *TP53* mutations in HGSC (47) as well as alterations in G1/S transition master regulators [RB1 deficiency (48) and *CCNE1* amplifications (49)] present the highly relevant molecular landscape for exploration of WEE1 and PKMYT1 co-inhibition as a treatment option. It is of interest to assess the potential of the

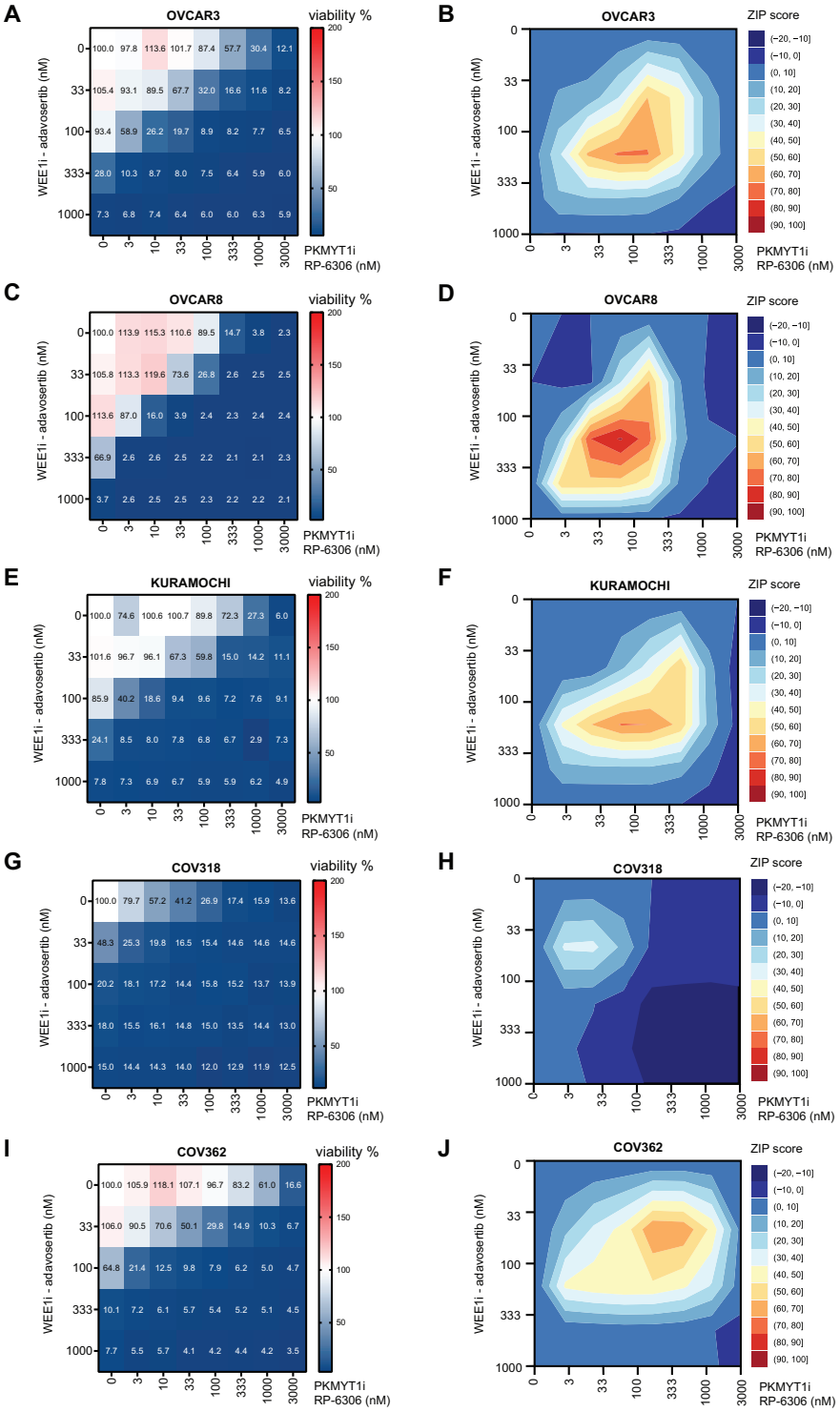

Figure 4. WEE1 and PKMYT1 co-inhibition kills a variety of high-grade ovarian serous adenocarcinoma cell lines regardless of their driver oncogenes. (**A**) Dose response matrix for cell viability upon 5-day treatment with adavosertib in combination with RP-6306 in OVCAR3 cells; data represent mean from triplicate. (**B**) Synergy ZIP scores corresponding to data in panel (A) presented a synergy landscape. A score $\geq$10 represents synergy and a score ≤ -10 represents antagonism. (**C**) Dose response matrix for cell viability upon 5-day treatment with adavosertib in combination with RP-6306 in OVCAR8 cells; data represent mean from triplicate. (**D**) Synergy ZIP scores corresponding to data in panel (C) presented a synergy landscape. (**E**) Dose response matrix for cell viability upon 5-day treatment with adavosertib in combination with RP-6306 in KURAMOCHI cells; data represent mean from triplicate. (**F**) Synergy ZIP scores corresponding to data in panel (E) presented a synergy landscape. A score $\geq$10 represents synergy and a score ≤ -10 represents antagonism. (**G**) Dose response matrix for cell viability upon 5-day treatment with adavosertib in combination with RP-6306 in COV318 cells; data represent mean from triplicate. (**H**) Synergy ZIP scores corresponding to data in panel (G) presented a synergy landscape. (**I**) Dose response matrix for cell viability upon 5-day treatment with WEE1i inhibitor adavosertib in combination with PKMYT1 inhibitor RP-6306 in COV362 cells; data represent mean from triplicate. (**J**) Synergy ZIP scores corresponding to data in panel (I) presented a synergy landscape.

A

Sample	Tumor cells origin	Patient Treatment	Mutations				CNV				Ploidy
			TP53	*BRCA1*	*BRCA2*	*RB1*	*RB1*	*CCNE1*	*KRAS*	*MYC*	
EOC989	omentum	NACT	miss + LOH	WT	WT	splicing + LOH	2	2	3	4	3.1
EOC172	ascites	NACT	miss + LOH	WT	WT	WT	1	2	2	5	2.0
EOC382	omentum	naive	stop + LOH	WT	WT	WT	2	8	3	3	3.5
EOC540	omentum	naive	miss + LOH	WT	WT	WT	1	4	7	7	2.9
EOC884	ascites	NACT	miss + LOH	WT	WT	WT	3	11	4	4	2.8

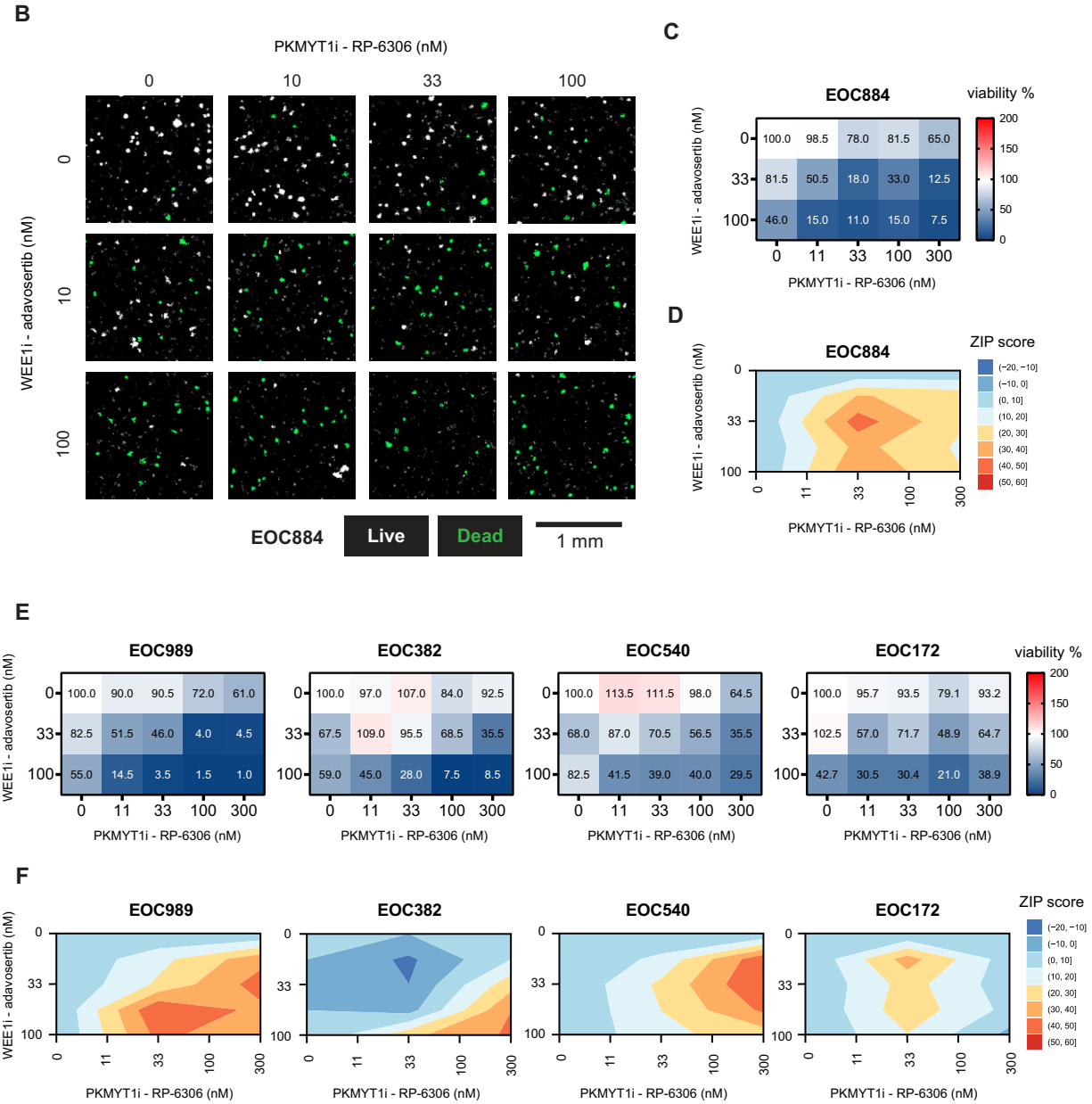

Figure 5. WEE1 and PKMYT1 co-inhibition kills patient-derived ovarian cancer organoids. (**A**) Characteristics of the selected set of long-term organoid cultures. NACT, neoadjuvant platinum-based chemotherapy. Mutations: fs, frameshift; stop, stop-gain; miss, missense mutation; splicing, splicing isoform mutation; LOH, loss of heterozygosity. Copy number columns indicate number of gene copies per cell; the numbers in red highlight the amplification of the gene. (**B**) Representative micrographs of HGSC organoids from patient EOC884. The organoids were treated with increasing doses of RP-6306 and adavosertib for 7 days. White masks label CellTox Green-negative live organoids and green masks label CellTox Green-positive dead organoids. Scale bar indicates 1 mm. (**C**) Quantification of the viability of EOC884 organoids after 7 days of the drug combination treatment illustrated in panel (B). Values in heat map cells present the percentage of live organoids relative to DMSO-treated control. Mean, $n = 3$.(**D**) ZIP synergy plots for adavosertib and RP-6306 interaction in the dose matrix viability testing in EOC884 organoids in panel (C). Interaction was classified as synergistic if ZIP score $\geq$10. (**E**) Quantification of the viability in panel of HGSC organoids after 7 days of the drug combination treatment illustrated in panel (B). Values in heat map cells present the percentage of live organoids relative to DMSO-treated control. Mean, $n = 3$. (**F**) ZIP synergy plots for adavosertib and RP-6306 interaction in the dose matrix viability testing in panel of HGSC (E). Interaction was classified as synergistic if ZIP score $\geq$10.

combination treatment to eradicate the residual tumour cells, which lose the sensitivity to the standard chemotherapeutics (50) and frequently are selected to restore the homologous recombination repair pathway (51), excluding the further possibility to use PARP inhibitors in the treatment. We have employed ovarian cancer organoids to represent three-dimensional cell culture models closely reflecting the primary tissue's biology and pathology. We observed a pronounced synergistic response to the combination in HGSC organoids established from residual tumour samples collected after a few cycles of chemotherapy (EOC884 and EOC989; Figure 5, and Supplementary Figure S4C and D). As the preclinical drug testing in organoids helps accurately predict the clinical treatment outcome (29,52,53,54), the observed efficacy of the multiple low-dose treatment with WEE1 and PKMYT inhibitors suggests that the respective tumours may have responded to the therapeutic combination. Hence, the combination may offer a treatment strategy to attenuate the relapses due to chemoresistant disease, which affects up to 70% of HGSC cases (1,3). Even though we focused mostly on ovarian cancer model systems, we have also shown that the multiple low-dose strategy can potentially be effective in other tumour types as indicated by our results in the U2OS cells of osteosarcoma origin. Collectively, our findings argue for a reduced focus on maximal tolerable dose of single targeted cancer drugs and suggest the use of drug combinations at low and non-toxic concentrations.

DATA AVAILABILITY

All data generated during this study are included in this article and its supplementary files. Raw microscopical data are available upon request.

SUPPLEMENTARY DATA

Supplementary Data are available at NAR Cancer Online.

ACKNOWLEDGEMENTS

We thank the members of CSS and KW laboratories and Repare Therapeutics for insightful comments; Repare Therapeutics for providing us with RP-6306; Shou Yun Yin (Repare Therapeutics) for performing the pharmacokinetic analysis; Department of Experimental Medicine (University of Copenhagen) for animal work; the core facilities at BRIC for assistance; BRIC's Core Facility for High-Content CRISPR Screens and Karolin Voßgröne for assistance with Echo 550 acoustic liquid handler; and J. Bartek laboratory (Danish Cancer Society) for BJ fibroblast HRAS(G12V) Tet ON cells.

FUNDING

Danish Cancer Society (R325-A18910-B224); Novo Nordisk Foundation (NNF22OC0079754).
Conflict of interest statement. None declared.

REFERENCES

1. Gadducci,A., Guarneri,V., Peccatori,F.A., Ronzino,G., Scandurra,G., Zamagni,C., Zola,P. and Salutari,V. (2019) Current strategies for the targeted treatment of high-grade serous epithelial ovarian cancer and relevance of BRCA mutational status. *J. Ovarian Res.*, **12**, 9.
2. Lisio,M.A., Fu,L., Goyeneche,A., Gao,Z.H. and Telleria,C. (2019) High-grade serous ovarian cancer: basic sciences, clinical and therapeutic standpoints. *Int. J. Mol. Sci.*, **20**, 952.
3. Pignata,S.C.C., Du Bois,A., Harter,P. and Heitz,F. (2017) Treatment of recurrent ovarian cancer. *Ann. Oncol.*, **28**, viii51–viii56.
4. Ray-Coquard,I., Mirza,M.R., Pignata,S., Walther,A., Romero,I. and du Bois,A. (2020) Therapeutic options following second-line platinum-based chemotherapy in patients with recurrent ovarian cancer: comparison of active surveillance and maintenance treatment. *Cancer Treat. Rev.*, **90**, 102107.
5. Chiappa,M., Guffanti,F., Bertoni,F., Colombo,I. and Damia,G. (2021) Overcoming PAPRPi resistance: preclinical and clinical evidence in ovarian cancer. *Drug Resist. Updates*, **55**, 100744.
6. Lheureux,S., Cristea,M.C., Bruce,J.P., Garg,S., Cabanero,M., Mantia-Smaldone,G., Olawaiye,A.B., Ellard,S.L., Weberpals,J.I., Wahner Hendrickson,A.E. *et al.* (2021) Adavosertib plus gemcitabine for platinum-resistant or platinum-refractory recurrent ovarian cancer: a double-blind, randomised, placebo-controlled, phase 2 trial. *Lancet*, **397**, 281–292.
7. McGowan,C.H. and Russell,P. (1993) Human Wee1 kinase inhibits cell division by phosphorylating p34cdc2 exclusively on Tyr15. *EMBO J.*, **12**, 75–85.
8. Watanabe,N., Broome,M. and Hunter,T. (1995) Regulation of the human WEE1Hu CDK tyrosine 15-kinase during the cell cycle. *EMBO J.*, **14**, 1878–1891.
9. Toledo,L.I., Altmeyer,M., Rask,M.B., Lukas,C., Larsen,D.H., Povlsen,L.K., Bekker-Jensen,S., Mailand,N., Bartek,J. and Lukas,J. (2013) ATR prohibits replication catastrophe by preventing global exhaustion of RPA. *Cell*, **155**, 1088–1103.
10. Dobbelstein,M. and Sorensen,C.S. (2015) Exploiting replicative stress to treat cancer. *Nat. Rev. Drug Discov.*, **14**, 405–423.
11. Toledo,L., Neelsen,K.J. and Lukas,J. (2017) Replication catastrophe: when a checkpoint fails because of exhaustion. *Mol. Cell*, **66**, 735–749.
12. Elbaek,C.R., Petrosius,V. and Sorensen,C.S. (2020) WEE1 kinase limits CDK activities to safeguard DNA replication and mitotic entry. *Mutat. Res.*, **819–820**, 111694.
13. Dillon,M.T., Good,J.S. and Harrington,K.J. (2014) Selective targeting of the G2/M cell cycle checkpoint to improve the therapeutic index of radiotherapy. *Clin. Oncol. (R. Coll. Radiol.)*, **26**, 257–265.
14. Shaltiel,I.A., Krenning,L., Bruinsma,W. and Medema,R.H. (2015) The same, only different—DNA damage checkpoints and their reversal throughout the cell cycle. *J. Cell Sci.*, **128**, 607–620.
15. Hirai,H., Iwasawa,Y., Okada,M., Arai,T., Nishibata,T., Kobayashi,M., Kimura,T., Kaneko,N., Ohtani,J., Yamanaka,K. *et al.* (2009) Small-molecule inhibition of Wee1 kinase by MK-1775 selectively sensitizes p53-deficient tumor cells to DNA-damaging agents. *Mol. Cancer Ther.*, **8**, 2992–3000.
16. Kong,A. and Mehanna,H. (2021) WEE1 inhibitor: clinical development. *Curr. Oncol. Rep.*, **23**, 107.
17. Martorana,F., Da Silva,L.A., Sessa,C. and Colombo,I. (2022) Everything comes with a price: the toxicity profile of DNA-damage response targeting agents. *Cancers (Basel)*, **14**, 953.
18. Caumanns,J.J., van Wijngaarden,A., Kol,A., Meersma,G.J., Jalving,M., Bernards,R., van der Zee,A.G.J., Wisman,G.B.A. and de Jong,S. (2019) Low-dose triple drug combination targeting the PI3K/AKT/mTOR pathway and the MAPK pathway is an effective approach in ovarian clear cell carcinoma. *Cancer Lett.*, **461**, 102–111.
19. Fernandes Neto,J.M., Nadal,E., Bosdriesz,E., Ooft,S.N., Farre,L., McLean,C., Klarenbeek,S., Jurgens,A., Hagen,H., Wang,L. *et al.* (2020) Multiple low dose therapy as an effective strategy to treat EGFR inhibitor-resistant NSCLC tumours. *Nat. Commun.*, **11**, 3157.
20. Ozkan-Dagliyan,I., Diehl,J.N., George,S.D., Schaefer,A., Papke,B., Klotz-Noack,K., Waters,A.M., Goodwin,C.M., Gautam,P., Pierobon,M. *et al.* (2020) Low-dose vertical inhibition of the RAF–MEK–ERK cascade causes apoptotic death of KRAS mutant cancers. *Cell Rep.*, **31**, 107764.

21. Liu,F., Stanton,J.J., Wu,Z. and Piwnica-Worms,H. (1997) The human Myt1 kinase preferentially phosphorylates Cdc2 on threonine 14 and localizes to the endoplasmic reticulum and Golgi complex. *Mol. Cell. Biol.*, **17**, 571–583.
22. Lundgren,K., Walworth,N., Booher,R., Dembski,M., Kirschner,M. and Beach,D. (1991) mik1 and wee1 cooperate in the inhibitory tyrosine phosphorylation of cdc2. *Cell*, **64**, 1111–1122.
23. Sheldrick,K.S. and Carr,A.M. (1993) Feedback controls and G2 checkpoints: fission yeast as a model system. *Bioessays*, **15**, 775–782.
24. Toledo,C.M., Ding,Y., Hoellerbauer,P., Davis,R.J., Basom,R., Girard,E.J., Lee,E., Corrin,P., Hart,T., Bolouri,H. *et al.* (2015) Genome-wide CRISPR–Cas9 screens reveal loss of redundancy between PKMYT1 and WEE1 in glioblastoma stem-like cells. *Cell Rep.*, **13**, 2425–2439.
25. Lewis,C.W., Bukhari,A.B., Xiao,E.J., Choi,W.S., Smith,J.D., Homola,E., Mackey,J.R., Campbell,S.D., Gamper,A.M. and Chan,G.K. (2019) Upregulation of Myt1 promotes acquired resistance of cancer cells to Wee1 inhibition. *Cancer Res.*, **79**, 5971–5985.
26. Szychowski,J., Papp,R., Dietrich,E., Liu,B., Vallee,F., Leclaire,M.E., Fourtounis,J., Martino,G., Perryman,A.L., Pau,V. *et al.* (2022) Discovery of an orally bioavailable and selective PKMYT1 inhibitor, RP-6306. *J. Med. Chem.*, **65**, 10251–10284.
27. Gallo,D., Young,J.T.F., Fourtounis,J., Martino,G., Alvarez-Quilon,A., Bernier,C., Duffy,N.M., Papp,R., Roulston,A., Stocco,R. *et al.* (2022) CCNE1 amplification is synthetic lethal with PKMYT1 kinase inhibition. *Nature*, **604**, 749–756.
28. Xuan,Z.H., Wang,H.P., Zhang,X.N., Chen,Z.X., Zhang,H.Y. and Gu,M.M. (2020) PKMYT1 aggravates the progression of ovarian cancer by targeting SIRT3. *Eur. Rev. Med. Pharmacol. Sci.*, **24**, 5259–5266.
29. Senkowski,W., Gall-Mas,L., Falco,M.M., Li,Y., Lavikka,K., Kriegbaum,M.C., Oikkonen,J., Bulanova,D., Pietras,E.J., Vossgrone,K. *et al.* (2023) A platform for efficient establishment and drug-response profiling of high-grade serous ovarian cancer organoids. *Dev. Cell*, https://doi.org/10.1016/j.devcel.2023.04.012.
30. Yadav,B., Wennerberg,K., Aittokallio,T. and Tang,J. (2015) Searching for drug synergy in complex dose-response landscapes using an interaction potency model. *Comput. Struct. Biotechnol. J.*, **13**, 504–513.
31. Ianevski,A., Giri,A.K. and Aittokallio,T. (2020) SynergyFinder 2.0: visual analytics of multi-drug combination synergies. *Nucleic Acids Res.*, **48**, W488–W493.
32. Wickham,H. (2009) In: *ggplot2: Elegant Graphics for Data Analysis (Use R!)*. Springer, Berlin, pp. 1–212.
33. Petrosius,V., Benada,J., Nielsen,O., Schoof,E.M. and Sorensen,C.S. (2023) Temporal phosphoproteomics reveals WEE1-dependent control of 53BP1 pathway. *iScience*, **26**, 105806.
34. Gaillard,H., Garcia-Muse,T. and Aguilera,A. (2015) Replication stress and cancer. *Nat. Rev. Cancer*, **15**, 276–289.
35. Macheret,M. and Halazonetis,T.D. (2015) DNA replication stress as a hallmark of cancer. *Annu. Rev. Pathol.*, **10**, 425–448.
36. Evangelou,K., Bartkova,J., Kotsinas,A., Pateras,I.S., Liontos,M., Velimezi,G., Kosar,M., Liloglou,T., Trougakos,I.P., Dyrskjot,L. *et al.* (2013) The DNA damage checkpoint precedes activation of ARF in response to escalating oncogenic stress during tumorigenesis. *Cell Death Differ.*, **20**, 1485–1497.
37. Maya-Mendoza,A., Ostrakova,J., Kosar,M., Hall,A., Duskova,P., Mistrik,M., Merchut-Maya,J.M., Hodny,Z., Bartkova,J., Christensen,C. *et al.* (2015) Myc and Ras oncogenes engage different energy metabolism programs and evoke distinct patterns of oxidative and DNA replication stress. *Mol. Oncol.*, **9**, 601–616.
38. Chen,Y.J., Dominguez-Brauer,C., Wang,Z., Asara,J.M., Costa,R.H., Tyner,A.L., Lau,L.F. and Raychaudhuri,P. (2009) A conserved phosphorylation site within the forkhead domain of FoxM1B is required for its activation by cyclin-CDK1. *J. Biol. Chem.*, **284**, 30695–30707.
39. Vassilev,L.T., Tovar,C., Chen,S., Knezevic,D., Zhao,X., Sun,H., Heimbrook,D.C. and Chen,L. (2006) Selective small-molecule inhibitor reveals critical mitotic functions of human CDK1. *Proc. Natl Acad. Sci. U.S.A.*, **103**, 10660–10665.
40. Chen,M., Linstra,R. and van Vugt,M. (2022) Genomic instability, inflammatory signaling and response to cancer immunotherapy. *Biochim. Biophys. Acta Rev. Cancer*, **1877**, 188661.
41. Krupina,K., Goginashvili,A. and Cleveland,D.W. (2021) Causes and consequences of micronuclei. *Curr. Opin. Cell Biol.*, **70**, 91–99.
42. Bulanova,D., Akimov,Y., Senkowski,W., Oikkonen,J., Gall-Mas,L., Timonen,S., Elmadani,M., Hynninen,J., Hautaniemi,S., Aittokallio,T. *et al.* (2022) A synthetic lethal dependency on casein kinase 2 in response to replication-perturbing drugs in RB1-deficient ovarian and breast cancer cells. bioRxiv doi: https://doi.org/10.1101/2022.11.14.516369, 16 November 2022, preprint: not peer reviewed.
43. Groelly,F.J., Fawkes,M., Dagg,R.A., Blackford,A.N. and Tarsounas,M. (2023) Targeting DNA damage response pathways in cancer. *Nat. Rev. Cancer*, **23**, 78–94.
44. Golder,A., Nelson,L., Tighe,A., Barnes,B., Coulson-Gilmer,C., Morgan,R.D., McGrail,J.C. and Taylor,S.S. (2022) Multiple-low-dose therapy: effective killing of high-grade serous ovarian cancer cells with ATR and CHK1 inhibitors. *NAR Cancer*, **4**, zcac036.
45. Halazonetis,T.D., Gorgoulis,V.G. and Bartek,J. (2008) An oncogene-induced DNA damage model for cancer development. *Science*, **319**, 1352–1355.
46. Taniguchi,H., Caeser,R., Chavan,S.S., Zhan,Y.A., Chow,A., Manoj,P., Uddin,F., Kitai,H., Qu,R., Hayatt,O. *et al.* (2022) WEE1 inhibition enhances the antitumor immune response to PD-L1 blockade by the concomitant activation of STING and STAT1 pathways in SCLC. *Cell Rep.*, **39**, 110814.
47. The Cancer Genome Atlas Research Network (2011) Integrated genomic analyses of ovarian carcinoma. *Nature*, **474**, 609–615.
48. Garsed,D.W., Alsop,K., Fereday,S., Emmanuel,C., Kennedy,C.J., Etemadmoghadam,D., Gao,B., Gebski,V., Gares,V., Christie,E.L. *et al.* (2018) Homologous recombination DNA repair pathway disruption and retinoblastoma protein loss are associated with exceptional survival in high-grade serous ovarian cancer. *Clin. Cancer Res.*, **24**, 569–580.
49. Karst,A.M., Jones,P.M., Vena,N., Ligon,A.H., Liu,J.F., Hirsch,M.S., Etemadmoghadam,D., Bowtell,D.D. and Drapkin,R. (2014) Cyclin E1 deregulation occurs early in secretory cell transformation to promote formation of fallopian tube-derived high-grade serous ovarian cancers. *Cancer Res.*, **74**, 1141–1152.
50. Bowtell,D.D., Bohm,S., Ahmed,A.A., Aspuria,P.J., Bast,R.C. Jr, Beral,V., Berek,J.S., Birrer,M.J., Blagden,S., Bookman,M.A. *et al.* (2015) Rethinking ovarian cancer II: reducing mortality from high-grade serous ovarian cancer. *Nat. Rev. Cancer*, **15**, 668–679.
51. Goel,N., Foxall,M.E., Scalise,C.B., Wall,J.A. and Arend,R.C. (2021) Strategies in overcoming homologous recombination proficiency and PARP inhibitor resistance. *Mol. Cancer Ther.*, **20**, 1542–1549.
52. de Witte,C.J., Espejo Valle-Inclan,J., Hami,N., Lohmussaar,K., Kopper,O., Vreuls,C.P.H., Jonges,G.N., van Diest,P., Nguyen,L., Clevers,H. *et al.* (2020) Patient-derived ovarian cancer organoids mimic clinical response and exhibit heterogeneous inter- and intrapatient drug responses. *Cell Rep.*, **31**, 107762.
53. Hill,S.J., Decker,B., Roberts,E.A., Horowitz,N.S., Muto,M.G., Worley,M.J. Jr, Feltmate,C.M., Nucci,M.R., Swisher,E.M., Nguyen,H. *et al.* (2018) Prediction of DNA repair inhibitor response in short-term patient-derived ovarian cancer organoids. *Cancer Discov.*, **8**, 1404–1421.
54. Maenhoudt,N., Defraye,C., Boretto,M., Jan,Z., Heremans,R., Boeckx,B., Hermans,F., Arijs,I., Cox,B., Van Nieuwenhuysen,E. *et al.* (2020) Developing organoids from ovarian cancer as experimental and preclinical models. *Stem Cell Rep.*, **14**, 717–729.